TÜBİTAK

Turkish Journal of Earth Sciences

http://journals.tubitak.gov.tr/earth/

Research Article

Turkish J Earth Sci
(2016) 25: 573-591

doi:10.3906/yer-1512-8

Geochemical characterization and palynological studies of some Agbada Formation deposits of the Niger Delta basin: implications for paleodepositional environments

Olajide Femi ADEBAYO[1], Segun Ajayi AKINYEMI[1,*], Henry Yemagu MADUKWE[1], Adeyinka Oluyemi ATURAMU[2], Adebayo Olufemi OJO[1]

[1]Department of Geology, Ekiti State University, Ado Ekiti, Nigeria

[2]Department of Geology, University of Leicester, Leicester, UK

Received: 14.12.2015 • **Accepted/Published Online:** 06.09.2016 • **Final Version:** 01.12.2016

Abstract: Forty-two ditch cutting samples of the KR-1 offshore well from depths of 9660 ft to 10,920 ft composited at 90-ft intervals were subjected to sedimentological, micropaleontological, and geochemical analyses using standard procedures and the laser ablation-induced coupled plasma mass spectrometry technique, respectively. Sedimentological analysis revealed the presence of glauconites and the rare occurrence of framboidal pyrites, indicative of deposition in a slightly anoxic marine environment. Palynomorph percentage distribution shows that there are more terrestrially derived miospores (dominated by *Zonocostites ramonae* (*Rhizophora* spp.), *Psilatricolporites crassus* (*Tabernaemontana crassa*), *Acrotichum aureum*, and *Laevigatosporites* sp.) than marine phytoplanktons. Rare occurrence of *Globoquadrina venezuelana*, *Globigerinoides promordius*, and *Globigerina* sp. denotes an Early Miocene age and proximal shelf. These indicate that the main environment of deposition in the KR-1 well is coastal to marginal marine consisting of coastal deltaic-inner neritic, made up of tidal channel and shoreface deposits. Geochemical results show that the average concentrations of considered rare earth elements are less than their concentrations in world average shale. Trace metal ratios (such as Th/Cr, Cr/Th, Th/Co, and Cr/Ni) suggest that the investigated sediments were derived from felsic source rocks. Rare earth element patterns (such as La/Yb, Gd/Yb, La/Sm, and Eu/Eu) and Th data established the felsic composition of the source rocks. Ratios of U/Th, Ni/Co, Cu/Zn, and V/Sc suggest a well-oxygenated bottom water condition. Estimated europium and cerium anomalies of the studied samples suggest an oxidizing environment of deposition. Nonetheless, the ratios of V/Cr suggest a range of environmental conditions. Moreover, ratios of V/(V+Ni) suggest the rare occurrence of suboxic to anoxic environments of deposition.

Key words: Sedimentology, palynomorphs, traces elements, rare earth element, environment of deposition, Niger Delta, Nigeria

1. Introduction

The Niger Delta basin is one of the sedimentary basins in Nigeria (Figure 1). It is an important basin because it contains large hydrocarbon resources. This makes Nigeria the most prolific oil producer in Sub-Saharan Africa, ranking as the third largest producer of crude oil in Africa and the tenth largest in the world. Nigeria's economy is predominantly dependent on its oil sector; oil supplies 95% of Nigeria's foreign exchange earnings and 80% of its budgetary revenues (Olayiwola, 1987; Adenugba and Dipo, 2013). This petroliferous nature has made the basin, for many years, the subject of continuous, consistent, and extensive geologic investigations both for academic and economic purposes (Adebayo, 2011). Intensive exploration and exploitation of hydrocarbon in the basin has been ongoing since the early 1960s due to the discovery of oil in commercial quantity in the Oloibiri-1 well in 1956 (Nwajide and Reijers, 1996). Biostratigraphy played an important role in the exploration of oil and gas in the Niger Delta basin. Microfossils were employed among other things to reconstruct the paleoenvironment of the studied sections. This is important because different depositional settings imply different reservoir qualities in terms of architecture, connectivity, heterogeneity, and porosity-permeability characteristics (Simmons et al., 1999).

Trace element abundances in sedimentary rocks have added significantly to our understanding of crustal evolution with rare earth element (REE) patterns and Th being particularly useful in determining provenance (Ganai and Rashid, 2015). The geochemical behavior of trace elements in modern organic-rich, fine-grained sedimentary rocks (i.e. shales) and anoxic basins has often been documented to determine paleoenvironmental conditions of deposition (Brumsack, 1989; Calvert and Pedersen, 1993; Warning and Brumsack, 2000; Algeo

* Correspondence: segun.akinyemi@eksu.edu.ng

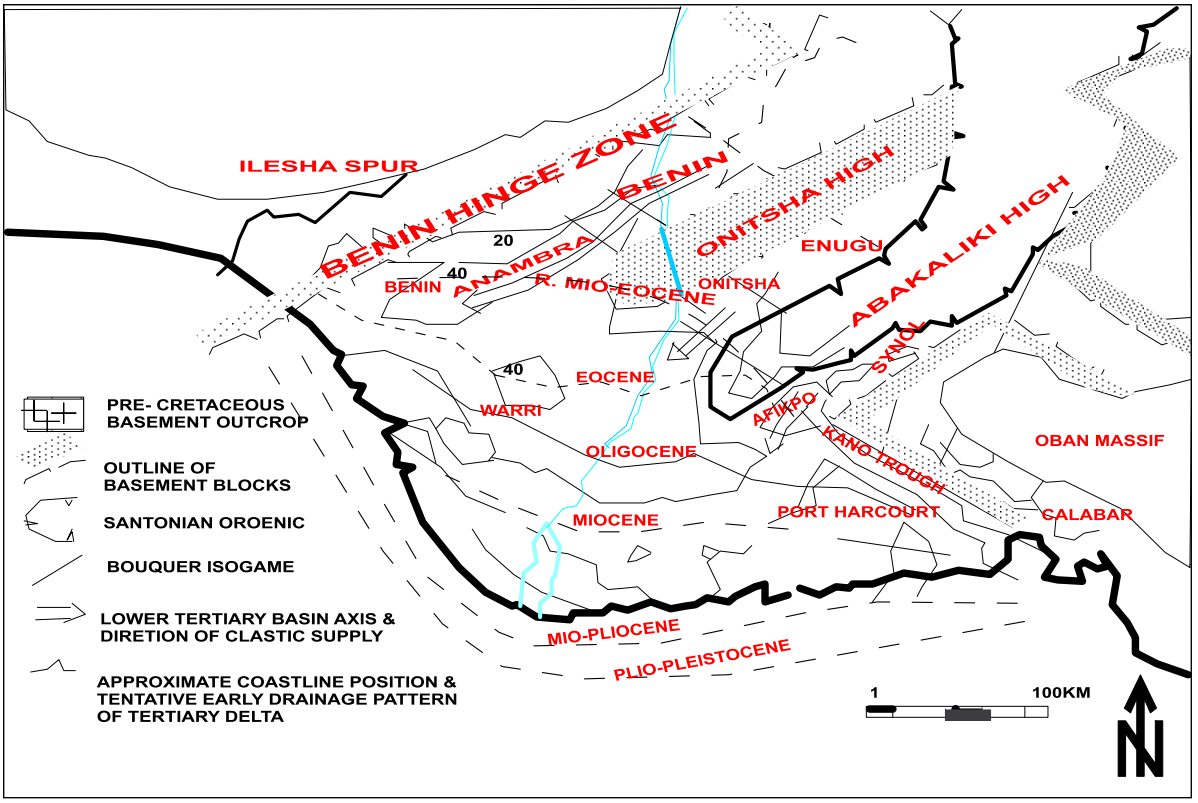

Figure 1. Geological map of the Niger Delta (Weber and Daukoru, 1975).

and Maynard, 2004). Redox-sensitive trace element (TE) concentrations or ratios are among the main extensively used indicators of redox conditions in modern and ancient sedimentary deposits (e.g., Calvert and Pedersen, 1993; Jones and Manning, 1994; Crusius et al., 1996; Dean et al., 1997, 1999; Yarincik et al., 2000; Morford et al., 2001; Pailler et al., 2002; Algeo and Maynard, 2004). Enrichments of redox-sensitive elements replicate the depositional environment of ancient organic carbon-rich sediments and sedimentary rocks as well and can consequently be used to reveal the likely paleodepositional conditions leading to their formation (Brumsack, 1980, 1986; Hatch and Leventhal, 1992; Piper, 1994). The degree of enrichment/depletion is usually based on the element/Al ratio in a sample, calculated relative to the respective element/Al ratio of a common standard material, e.g., average marine shale (Turekian and Wedepohl, 1961). The purpose of this paper is to interpret the paleoenvironmental changes during the deposition of the sediments in the studied section of the Niger Delta basin. To achieve the objective, a multidisciplinary approach combining sedimentological features and palynological and geochemical analyses was employed.

2. The geologic setting of the basin

The present-day Niger Delta Complex is situated on the continental margin of the Gulf of Guinea in the southern part of Nigeria. It lies between longitudes 4 °E and 8.8 °E and latitudes 3 °N and 6 °N (Figure 1).The onshore portion of the basin is delineated by the geology of southern Nigeria and southwestern Cameroon. It is bounded in the north by outcrops of the Anambra Basin and the Abakaliki Anticlinorium, and delimited in the west by the Benin Flank, a northeast-southwest trending hinge line south of the West African basement massif. The Calabar Flank, a hinge line bordering the Oban massif, defines the northeastern boundary. The offshore boundary of the basin is defined by the Cameroon volcanic line to the east and the eastern boundary of the Dahomey Basin (the eastern-most West African transform-fault passive margin) to the west. The evolution of the delta is controlled by pre- and synsedimentary tectonics as described by Evamy et al. (1978), Ejedawe (1981), Knox and Omatsola (1987), and Stacher (1995). It is a large arcuate delta covering an area of about 300,000 km^2 (Kulke, 1995), with a sediment volume of 500,000 km^3 (Hospers, 1965) and a sedimentary thickness of over 10 km in the basin depocenter (Kaplan et al., 1994).

The evolution of the basin has been linked to that of a larger sedimentary complex called the Benue-Abakaliki Trough. The trough, a NE-SW trending aborted rift basin with folded sedimentary fill, runs obliquely across Nigeria (Figure 1). The Niger Delta basin is actually the youngest and the southernmost subbasin in the trough (Murat, 1972; Reijers et al., 1997).

The evolution of the trough, which began in the Cretaceous, during the opening of the South Atlantic, led to the separation of the African and South American plates. The tectonic framework of the continental margin along the western coast of Africa is controlled by Cretaceous fracture zones expressed as trenches and ridges in the deep Atlantic. The fracture zone ridges subdivided the margin into individual basins and, in Nigeria, form the boundary faults of the Cretaceous Benue-Abakaliki Trough, which cuts far into the West African Shield. The rifting greatly diminished in the Late Cretaceous in the Niger Delta region (Ako et al., 2004). A well section through the Niger Delta basin generally displays three vertical lithostratigraphic subdivisions, namely a prodelta lithofacies, a delta front lithofacies, and upper delta top facies (Nwajide and Reijers, 1996). These lithostratigraphic units correspond respectively to the Akata Formation (Paleocene-Recent), Agbada Formation (Eocene-Recent), and Benin Formation (Oligocene-Recent) (Short and Stauble, 1967).

3. Materials and methods

Forty-two ditch cutting samples of the KR-1 offshore well (Figure 2) were taken from depths of 9660 to 10,920 ft at 90-ft interval (Figure 3). These were processed and analyzed for sedimentological, palynological, micropaleontological, and geochemical studies.

3.1. Sedimentological analysis

The samples were subjected to sedimentological analysis using visual inspection and a binocular microscope. Physical characteristics such as color, texture, hardness, fissility, and rock types were noted. Dilute HCl (10%) was added to identify the calcareous samples. Fossil contents, presence of accessory minerals, and postdepositional effects such as ferruginization were determined.

3.2. Palynological preparation

Ten grams of each dry sample was crushed into small fractions between 0.25 mm and 2.5 mm. Standard palynological processing procedures were employed (Faegri and Iversen, 1989; Wood et al., 1996). These included the digestion of the mineral matrix using dilute HCl for carbonates and concentrated HF for silicates. Removal of the fluoride gel (formed during the HF treatment) was done using hot concentrated HCl and wet sieving the residue using a 10-µm polypropylene Estal Mono sieve. The residues were oxidized and inorganic materials were separated from the organic ones using $ZnCl_2$ of specific gravity 2.0. Slides were mounted using Norland adhesive mounting medium and dried under UV light. One slide per sample was analyzed under the optical microscope and the photomicrographs of well-preserved palynomorph specimens were taken using an Olympus CH30 transmitted light microscope (Model CH30RF200) with an attached camera. Palynomorph identifications were done using the works of Germeraad et al. (1968) and Evamy et al. (1978) (i.e. Shell Oil Company Scheme, 1978). The data were plotted using *StrataBugs* software at 1:5000 scale with depth on the y-axis and the identified taxa on the x-axis.

3.3. Foraminiferal preparation

Twenty-five grams of each sample was processed for their foraminiferal content using the standard preparation techniques. The weighed samples were soaked in kerosene and left overnight to disaggregate, followed by soaking in detergent solution overnight. The disaggregated samples were then washed-sieved under running tap water over a 63-µm mesh sieve. The washed residues were then dried over a hot electric plate and sieved (when cooled) into three main size fractions, namely coarse, medium, and fine (250-, 150-, and 63-µm meshes). Each fraction was examined under a binocular microscope. All the foraminifera, ostracodes, shell fragments, and other microfossils observed were picked with the aid of a picking needle and counted. Foraminifera identification was made to genus and species levels where possible using the taxonomic scheme of Loeblich and Tappan (1964) and other relevant foraminiferal literature such as the works of Fayose (1970), Postuma (1971), Petters (1979a, 1979b, 1982), Murray (1991), and Okosun and Liebau (1999).

3.4. XRF and LA-ICPMS analyses

The pulverized ditch cutting samples were analyzed with X-ray fluorescence (XRF) and laser ablation-induced coupled plasma mass spectrometry (LA-ICPMS) techniques. The elemental data for this work were acquired using XRF and LA-ICPMS analyses.

The analytical procedures were as follows:

Pulverized ditch cutting samples were analyzed for major elements using an Axios instrument (PANalytical) with a 2.4-kW Rh X-ray tube. The same set of samples was further analyzed for trace elements using LA-ICPMS instrumental analysis. LA-ICPMS is a powerful and sensitive analytical technique for multielement analysis. The laser was used to vaporize the surface of the solid sample, while the vapor and any particles were then transported by the carrier gas flow to the ICP-MS. The detailed procedures for sample preparation for both analytical techniques are reported below.

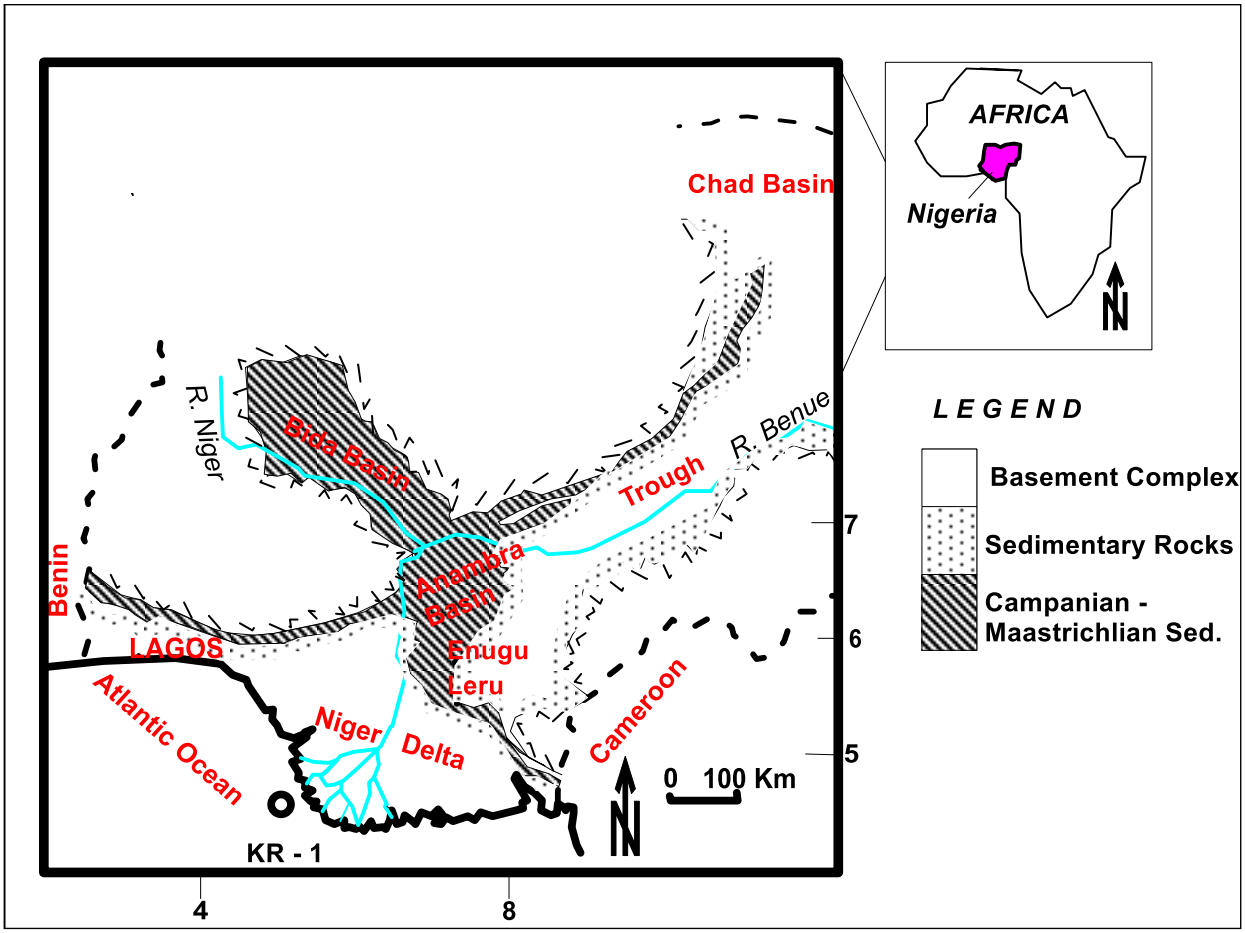

Figure 2. Simplified geologic map of Nigeria and location of KR-1 well (Adebayo et al., 2015b).

3.4.1. Fusion bead method for major element analysis

- Weigh 1.0000 ± 0.0009 g of milled sample.
- Place in oven at 110 °C for 1 h to determine H_2O+.
- Place in oven at 1000 °C for 1 h to determine LOI.
- Add 10.0000 ± 0.0009 g of Claisse flux and fuse in M4 Claissefluxer for 23 min.
- Add 0.2 g of $NaCO_3$ to the mix and preoxidize the sample+flux+$NaCO_3$ at 700 °C before fusion.
- Flux type: Ultrapure Fused Anhydrous Li-Tetraborate-Li-Metaborate flux (66.67% $Li_2B_4O_7$ + 32.83% $LiBO_2$) and releasing agent Li-iodide (0.5% LiI).

3.4.2. Pressed pellet method for trace element analysis

- Weigh 8 ± 0.05 g of milled powder.
- Mix thoroughly with 3 drops of Mowiol wax binder.
- Press pellet with pill press to pressure of 15 t.
- Dry in oven at 100 °C for 30 min. before analyzing.

These analytical methods yielded data for 11 major elements, reported as oxide percent by weight [SiO_2, TiO_2, Al_2O_3, Fe_2O_3, MgO, MnO, CaO, Na_2O, K_2O, Cr_2O_3, and P_2O_5] and 21 trace elements [Ni, Cu, Zn, Ga, Rb, Sr, Y, Zr, Nb, Co, V, Pb, Th, U, Ti, Cr, Ba, La, Ce, Nd, and P] reported as mg/kg (ppm).

4. Results and discussion

4.1. Sedimentological analysis

Lithologically, the sequence is characterized by the alternation of shale and sandy shale facies (Figure 3). The shales are light gray, fissile, effervescent and slightly ferruginized while the sandy shales are light gray and ferruginous. These sediments contain muscovite flakes. There are few to common occurrences of glauconite while pyrite and shell fragments are rare to few. Quartz grains within the sediments vary from fine to medium, subangular to well-rounded and moderately sorted.

4.2. Palynological assemblage

Palynomorph preservation in the analyzed sediments is fairly good with high concentration and diversity (see Figures 4 and 5). All the samples yielded common to

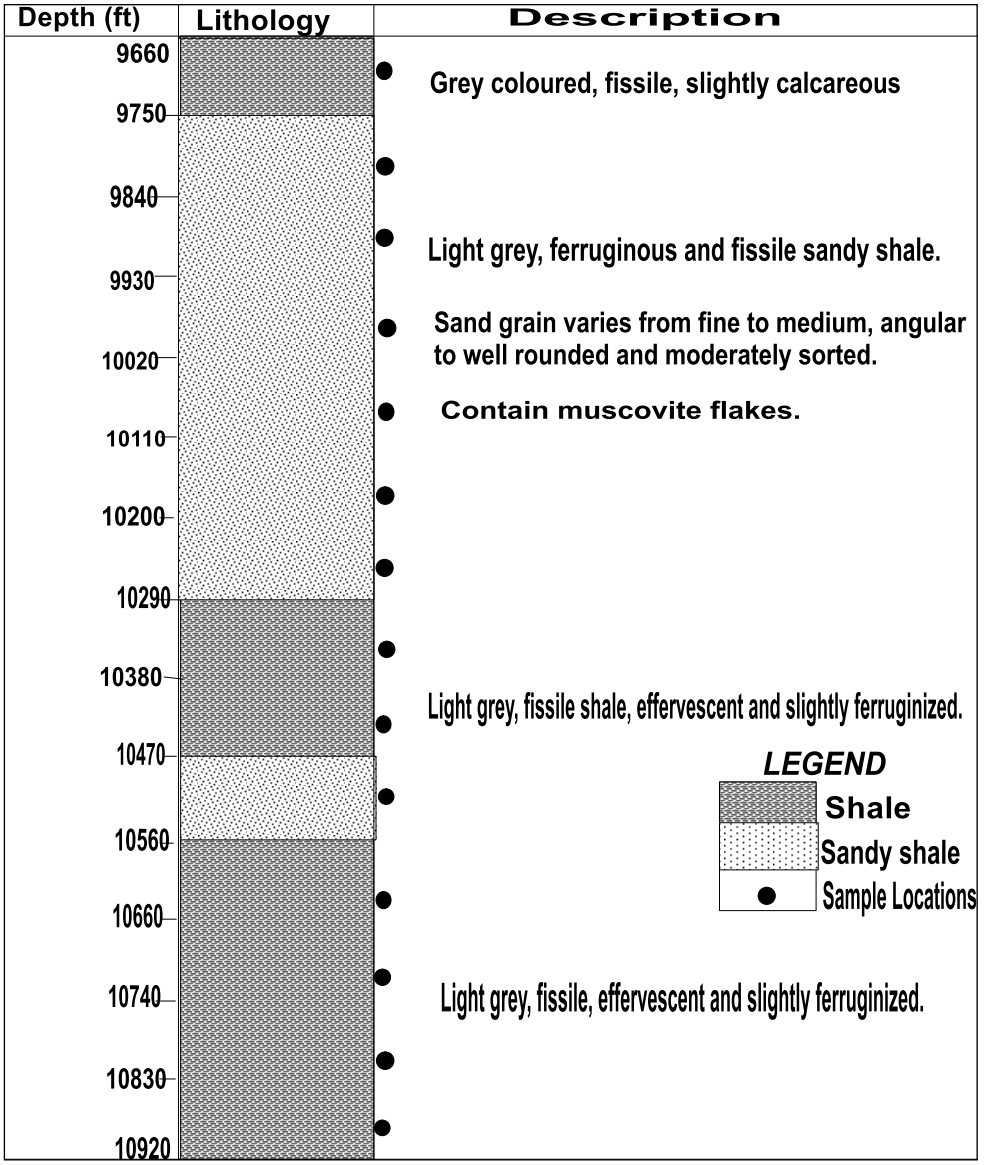

Figure 3. The lithology of the KR-1 well (after Adebayo et al., 2015b).

abundant assemblages that range from moderate to well preserved. Dinoflagellate cysts are sporadically present and range in abundance from very rare to few and do not occur in all the samples.

There are 256 pollen grains, 220 spores, 231 *Botryococcus* and *Pediastrum*, 9 dinoflagellate cysts, and 3 microforaminiferal wall linings, making a total of 719 recovered palynomorphs. The assemblage is dominated by angiospermous pollen with an equally significant occurrence of pteridophyte spores. The angiosperms consist mainly of *Tricolporites*, *Tetraporites*, and *Monoporites* while *Laevigatosporites*, *Verrucatosporites*, and *Polypodiaceoisporites* are the dominant pteridophyte spores (Figures 4 and 5). The biostratigraphically important palynomorphs recovered from the well are *Zonocostites ramonae* (*Rhisophora* sp.), *Psilatricolporites crassus* (*Tabermaemontana* sp.), *Pachydermites diederixi* (*Symphonia globulifera*), *Retitricolporites irregularis* (*Amanoa* sp.), *Praedapollis africanus*, and *Verrucatosporites usmensis* (*Polypodium* sp.) (Figures 4 and 5). The palynomorph assemblage as a whole shows strong similarities with those previously identified in the San Jorge Gulf Basin, southern Patagonia, Argentina (Palamarczuk and Barreda, 1998), and especially those from the Mazarredo Subbasin (Barreda and Palamarczuk, 2000), dated as Early Miocene and Latest Oligocene-Early Miocene, respectively. The KR-1 well assemblage is also closely comparable to the Early Miocene interval

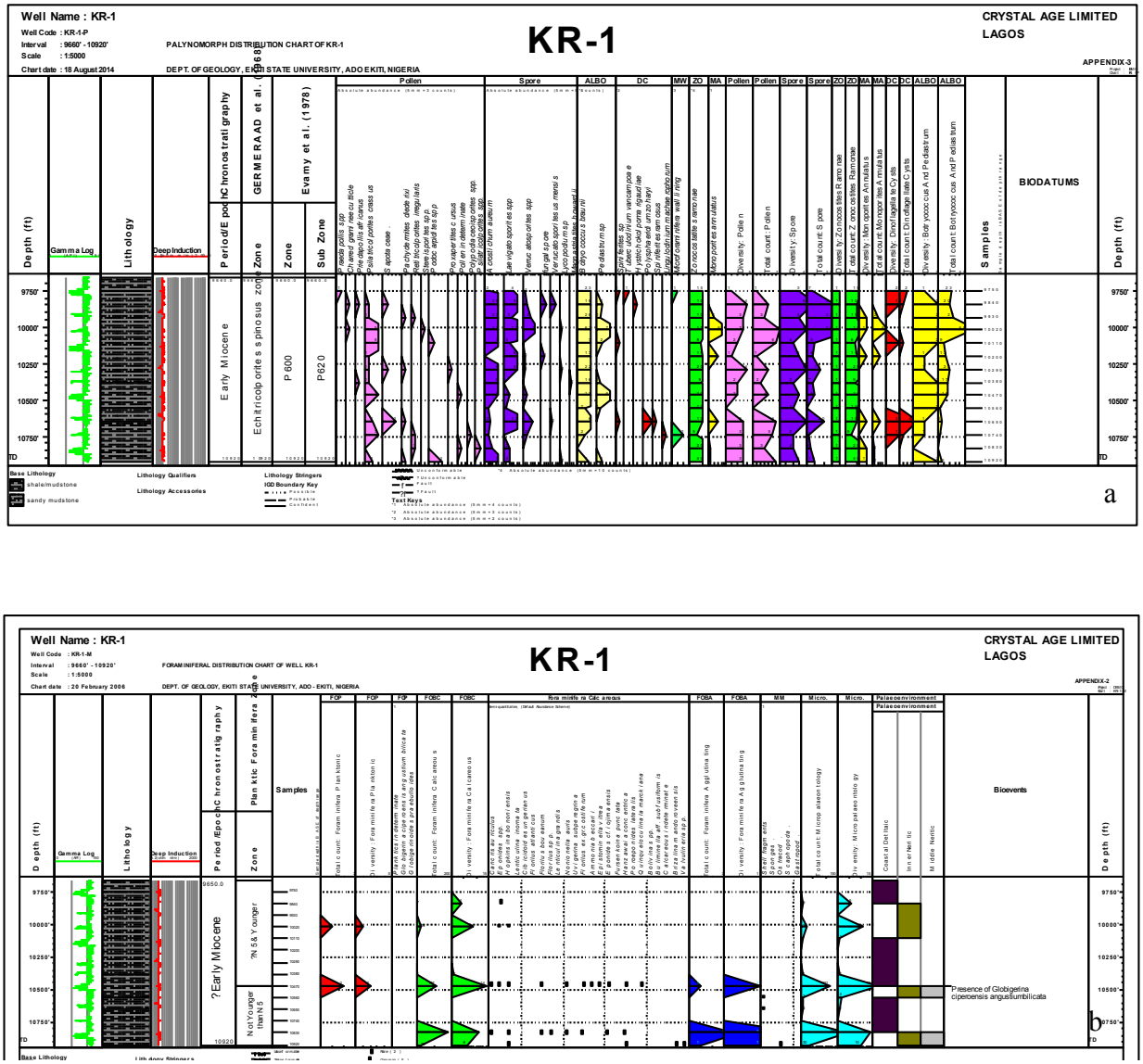

Figure 4. Chart of recovered (a) palynomorph and (b) foraminiferal assemblages from the investigated intervals from KR-1 well, Niger Delta (Adebayo et al., 2015b).

of coeval tropical-subtropical South American and Asian palynological assemblages (Graham, 1977; Kogbe and Sowunmi, 1980; Demchuk and Moore, 1993). This palynofloral association, the acme (or highest appearance datum, HAD) of some of the few recovered dinoflagellate cysts (*Lingulodinium machaerophorum*, *Polysphaeridium zoharyi*, *Hystrichokopoma rigaudiase*) among the taxa found in the rocks of Miocene age (El-Beialy et al., 2005), and the absence of Eocene and Oligocene forms such as *Crassoretitriletes vanraadshooveni*, *Bombacacidites* sp., *Operculodinium xanthium*, and *Thalassiphora pelagica* support the assignment of Early Miocene age.

4.3. Paleoenvironment of deposition

The reconstruction of the depositional environment of the studied well is based on some parameters such as palynomorph assemblage, abundance, diversity, and frequency distribution, as well as the relative abundance of *Zonocostites ramonae* to *Monoporites annulatus*, freshwater algae, organic wall microplanktons, lithologic characters, and accessory mineral contents. Environmentally

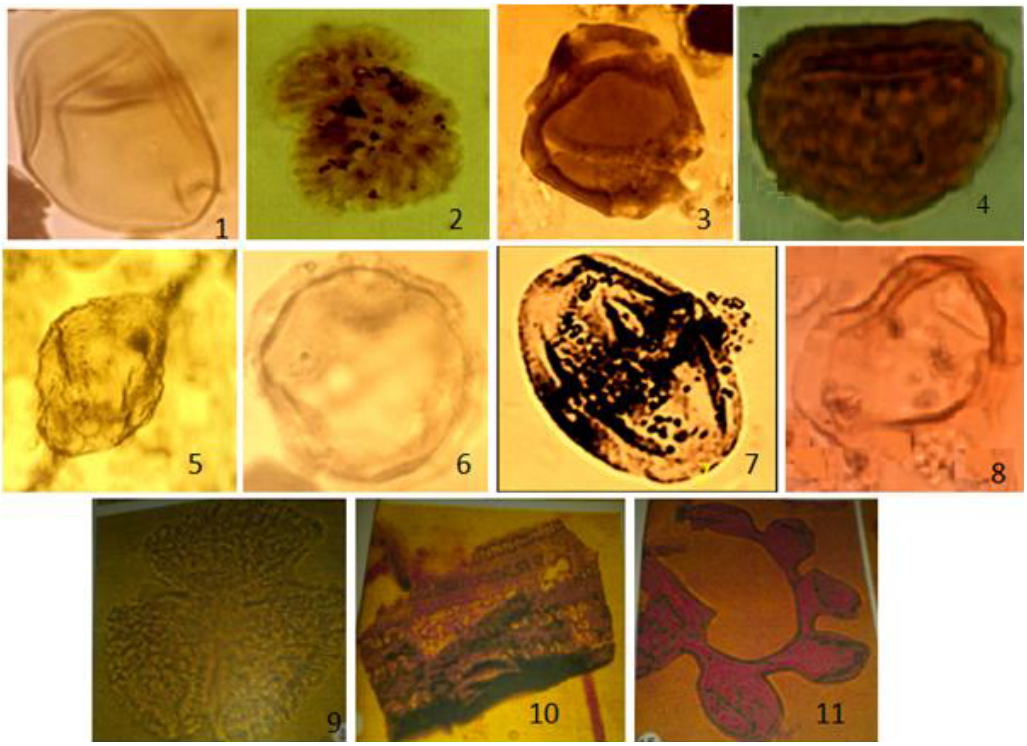

Figure 5. Plates of recovered palynomorphs from the investigated intervals from the KR-1 well (1000×). **1.** *Laevigatosporites* sp.; **2.** *Botryococcus braunii* Kützing, 1849; **3.** *Pachydermitesdiederixi* Germeraad, Hopping & Muller, 1968; **4.** *Verrucatosporites* sp.; **5.** *Palaeocystodinum* sp.; **6.** *Monoporites annulatus* van der Hammen, 1954; **7.** Sapotaceae; **8.** *Psilatricolporites crassus* van der Hammen & Wijmstra 1964; **9.** *Retitricolporites irregularis* van der Hammen & Wijmstra, 1964; **10.** charred Gramineae; **11.** microforaminiferal wall lining.

important marker species such as *Zonocostites ramonae* (mangrove pollen), *Monoporites annulatus* (Poaceae pollen suggesting open vegetation found in coastal Savannah), *Magnastriatites howardi* (a small aquatic fern of alluvial plain and coastal swamps), *Pachydermites diederixi* (an angiosperm of coastal swamps), foraminiferal wall linings, and dinocysts are recovered. Lithologically, glauconite and pyrite are the most important accessory minerals in the studied well that can be used for environmental deductions. Glauconite forms only as an authigenic mineral during the early stage of the diagenesis of marine sediments. It is extremely susceptible to subaerial weathering and is not known as a reworked second cycle detrital mineral (Selley, 1976). The presence of glauconite in the sandy shales therefore indicates a marine origin. On the other hand, rare occurrence of pyrite in the shale bodies probably suggests a reducing condition during deposition.

The studied sequence can be categorized into three sections based on significant changes in the occurrence of the recovered taxa (Figure 4). The lowermost section, which lies between depths of 10,920 and 10,560 ft, constituted a paleoecological zone. It is characterized by the appreciable occurrence of organic wall microplanktons such as foraminiferal wall linings and dinocysts (*Palaeocystodinum* spp.), uphole decrease in the population of *Monoporites annulatus*, rare occurrence of *Botryococcus braunii*, and the paucity of fresh water forms represented by *Pediastrum* (Figures 4 and 5). This section is assigned to a marginal marine environment (Sarjeant, 1974; Durugbo, 2013). The depth between 10,560 and 9930 ft belongs to a continental-mangrove environment based on the dominance of terrestrially derived taxa (*Psiltricolporites crassus* and *Pachydermites diederixi*), the acme of *Zonocostites ramonae*, and the absence or rarity of microplanktons. The topmost section, which lies between 9930 and 9750 ft, is a mixed environment that ranges from back-mangrove to brackish water swamp to marshes. Though this section of the well is dominated by *Botryococcus braunii* and *Zonocostites ramonae*, the significant presence of *Psilatricolporites crassus* and *Acrotichum aureum* (similar to *Deltoidospora adriennis*) (Figures 4 and 5) and the occurrence of microplanktons enable the suggestion of back-mangrove-brackish water swamp-marshes (Tomlinson, 1986; Thanikaimoni, 1987).

4.4. Trace element/Al ratios and enrichments

The enrichment factor (EF) for an individual element is equal to $(element/Al)_{sample}$ / $(element/Al)_{shale}$, where the

ratio in the numerator is that for the shale in question and the ratio in the denominator is that for a "typical" shale (using data from Wedepohl, 1971, 1991). Any relative enrichment is then expressed by EF > 1, whereas depletion elements have EF < 1. This approach has been used by various authors to evaluate trace-element enrichments in modern and ancient sediments (e.g., Calvert and Pedersen, 1993; Arnaboldi and Meyers, 2003; Rimmer, 2004; Brumsack, 2006). Generally, comparisons of V/Al ratios in the Agbada Formation samples with world average shale (Wedepohl, 1971) show high enrichment factors (EF_V = 5.74–1.15) at some depth intervals such as 9660–9750 ft, 9750–9840 ft, 9840–9930 ft, and 9930–10,020 ft (Table 1). In contrast, other investigated intervals were marked by low enrichment factors (EF_V = 0.40–0.05). Compared with average shale, Mo/Al ratios in the studied Agbada Formation samples show high enrichment factors (EF_{Mo} = 115.45–5.56) in all the investigated depth intervals. The observed variability in Mo/Al and V/Al ratios in the studied Agbada Formation samples are indicative of a mixed environment of deposition (i.e. paralic setting). Compared with world average shale, Ni/Al ratios in the Agbada Formation samples show high enrichment factors (EF_{Ni} = 5.21–1.21) at 9660–9750 ft, 9750–9840 ft, 9840–9930 ft, and 9930–10,020 ft depth intervals (Table 1). Alternatively, other investigated depth intervals show low enrichment factors (EF_{Ni} = 0.81–0.27). In comparison with the world average shale, Co/Al ratios in the studied samples show high enrichment factors (EF_{Co} = 14.56–1.64). Variability in the enrichment of Ni/Al and Co/Al ratios in the Agbada Formation samples indicate a mixed environment of deposition. U/Al ratios compared with average shale show high enrichment factors (EF_U = 5.28–1.11) in samples taken at depth intervals such as 9660–9750 ft, 9750–9840 ft, 9840–9930 ft, 9930–10,020 ft, 10,650–10,740 ft, 10,740–10,830 ft, and 10,830–10,920 ft (Table 1). Conversely, other investigated depth intervals show low enrichment factors (EF_U = 0.82–0.20). Compared with average shale, Cr/Al ratios show high enrichment factors (EF_{Cr} = 12.16–0.52), with the exception of the sample taken at the depth interval of 10,020-10,110 ft. Lower U/Al and Cr/Al ratios imply oxic bottom water conditions during deposition. Compared with world average shale, Sr/Al ratios in the Agbada Formation samples show high enrichment factors (EF_{Sr} = 4.60–1.01) at 10,650–10,740 ft, 10,740–10,830 ft, 10,830–10,920 ft, 9840–9930 ft, and 9930–10,020 ft depth intervals. Conversely, low enrichment factors (EF_{Sr} = 0.99–0.19) were observed in other investigated depth intervals. Ba/Al ratios in the studied samples compared with world average shale show high enrichment factors (EF_{Ba} = 54.71–1.31) in all the investigated depth intervals. Furthermore, a relatively high enrichment of Ba/Al and Sr/Al ratios suggest well-oxygenated bottom water conditions during deposition. The Cu/Al ratios in Agbada Formation samples compared with world average shale show high enrichment factors (EF_{Cu} = 6.97–1.64) at 10,380–10,470 ft, 10,650–10,740 ft, 10,740–10,380 ft, 10,380–10,920 ft, 9660–9750 ft, 9750–9840 ft, 9840–9930 ft, and 9930–10,020 ft depth intervals. Other investigated depth intervals show low enrichment factors (EF_{Cu} = 0.95–0.38). Zn/Al ratios in the studied samples compared with world average shale show high enrichment factors (EF_{Zn} = 12.92–0.79) with the exception of the sample taken at the 10020–10110 ft depth interval. Compared with world average shale, Pb/Al ratios for all samples show high enrichment factors (EF_{Pb} = 18.35–0.80), with the exception of samples taken at 10,020–10,110 ft and 10,200–10,290 ft depth intervals.

Going by the world average shale standard, Rb/Al ratios show evidence of low enrichment factors (EF_{Rb} = 3.34–0.10) with the exception of the sample taken at the 9660–9750 ft depth interval. Similarly, compared with world average shale, the Y/Al ratios in Agbada Formation samples show low enrichment factors (EF_Y = 4.38–1.04). Alternatively, low enrichment factors (EF_Y = 0.98–0.09) were obtained in samples taken at 9660–9750 ft, 9840–9930 ft, 9930–10,020 ft, 10,650–10,740 ft, and 10,740–10,830 ft depth intervals. Zr/Al ratios in Agbada Formation samples compared with world average shale show high enrichment factors (EF_{Zr} = 11.42–0.92), with the exception of the sample taken at the 10,020–10,110 ft depth interval. The studied Agbada Formation samples exhibit different degrees of trace-element enrichment, with the approximate order of enrichment relative to world average shale as follows: Mo > Ba > Pb > Cr > Co > Zn > Zr > Cu > V > U > Ni > Sr > Rb.

4.5. Provenance and paleoredox conditions

Armstrong-Altrin et al. (2004) revealed that low contents of Cr imply a felsic provenance, and high levels of Cr and Ni are essentially found in sediments derived from ultramafic rocks. Nickel concentrations are lower in the Agbada Formation sediments compared with world average shale (WSA) (Table 2), but chromium shows higher contents. Accordingly, the low Cr/Ni ratios in Agbada Formation samples are between 1.32 and 10.93. This indicates that felsic components were the major components among the basement complex source rocks. Some authors showed that ratios such as La/Sc, Th/Sc, Th/Co, and Th/Cr are significantly different in felsic and basic rocks and may possibly allow constraints on the average provenance composition (Wronkiewicz and Condie, 1990; Cullers, 1994, 1995, 2000; Cox et al., 1995; Cullers and Podkovyrov, 2000; Nagarajan et al., 2007). The ratios of Th/Cr (~0.03–0.09; average = ~0.05), Cr/Th (~10.70–30.64; average = ~20.37), Th/Co (~0.01–0.48; average = ~0.25), and Cr/Ni (~1.32–10.93; average = ~5.13) (Table 3) imply that the Agbada Formation sediments recovered from the KR-1 well were derived from felsic source

Table 1. Trace element ratios and enrichments in the Agbada Formation Sediments compared to world average shale (WSA) (Wedepohl, 1971).

Element	WSA	9660–9750 ft	9750–9840 ft	9840–9930 ft	9930–10,020 ft	10,020–10,110 ft	10,110–10,200 ft
Ni (ppm)	68	46.25	32.92	30.60	36.28	18.17	23.77
(Ni/Al)*104	7.7	40.15	9.73	10.89	9.99	2.04	2.85
EF		5.21	1.26	1.41	1.30	0.27	0.37
Co (ppm)	19	35.22	125.82	51.60	53.42	149.73	104.40
(Co/Al)*104	2.1	30.57	37.17	18.36	14.71	16.85	12.52
EF		14.56	17.70	8.74	7.01	8.02	5.96
Cu (ppm)	45	40.97	32.68	23.53	37.58	17.07	29.29
(Cu/Al)*104	5.1	35.56	9.65	8.37	10.35	1.92	3.51
EF		6.97	1.89	1.64	2.03	0.38	0.69
Zn (ppm)	95	163.73	170.23	196.74	280.27	77.06	165.94
(Zn/Al)*104	11	142.12	50.29	70.02	77.21	8.67	19.90
EF		12.92	4.57	6.37	7.02	0.79	1.81
V (ppm)	130	99.13	57.92	66.57	74.24	25.74	50.14
(V/Al)*104	15	86.05	17.11	23.69	20.45	2.90	6.01
EF		5.74	1.14	1.58	1.36	0.19	0.40
Cr (ppm)	90	142.85	150.93	135.35	196.18	46.71	100.47
(Cr/Al)*104	10.2	124.00	44.59	48.17	54.04	5.26	12.05
EF		12.16	4.37	4.72	5.30	0.52	1.18
Ba (ppm)	580	896.83	1063.47	515.00	556.06	766.98	3455.12
(Ba/Al)*104	66	778.49	314.17	183.29	153.18	86.30	414.36
EF		11.80	4.76	2.78	2.32	1.31	6.28

Table 1. (Continued).

Element	WSA	9660–9750 ft	9750–9840 ft	9840–9930 ft	9930–10,020 ft	10,020–10,110 ft	10,110–10,200 ft	10,200–10,290 ft
Rb (ppm)	140	61.60	31.90	36.73	41.58	14.02	32.27	25.40
(Rb/Al)*104	16	53.47	9.42	13.07	11.45	1.58	3.87	3.11
EF		3.34	0.59	0.82	0.72	0.10	0.24	0.19
Sr (ppm)	300	180.24	114.33	113.34	124.33	57.11	150.23	87.92
(Sr/Al)*104	34	156.45	33.77	40.34	34.25	6.43	18.02	10.77
EF		4.60	0.99	1.19	1.01	0.19	0.53	0.32
Zr (ppm)	160	236.75	185.52	195.99	208.18	147.83	250.34	179.02
(Zr/Al)*104	18	205.51	54.81	69.75	57.35	16.63	30.02	21.93
EF		11.42	3.04	3.88	3.19	0.92	1.67	1.22
Pb (ppm)	22	23.48	15.96	23.69	35.42	17.70	21.82	18.74
(Pb/Al)*104	2.5	20.38	4.71	8.43	9.76	1.99	2.62	2.30
EF		8.15	1.89	3.37	3.90	0.80	1.05	0.92
U (ppm)	3.7	2.56	1.78	1.96	2.07	0.76	1.59	1.20
(U/Al)*104	0.42	2.22	0.52	0.70	0.57	0.09	0.19	0.15
EF		5.28	1.25	1.66	1.35	0.20	0.45	0.35
Mo (ppm)	1	13.30	10.68	7.77	12.86	4.94	5.69	4.70
(Mo/Al)*104	0.1	11.55	3.16	2.76	3.54	0.56	0.68	0.58
EF		115.45	31.55	27.64	35.41	5.56	6.82	5.76
Y (ppm)	41	23.22	13.12	15.40	17.38	3.60	10.82	8.67
(Y/Al)*104	4.6	20.15	3.87	5.48	4.79	0.41	1.30	1.06
EF		4.38	0.84	1.19	1.04	0.09	0.28	0.23

Table 1. (Continued).

Element	WSA	10,290–10,380 ft	10,380–10,470 ft	10,470–10,560 ft	10,560–10,650 ft	10,650–10,740 ft	10,740–10,830 ft	10,830–10,920 ft
Ni (ppm)	68	36.60	52.90	41.83	41.82	39.77	57.15	54.48
(Ni/Al)*104	7.7	4.52	6.23	4.96	5.04	9.68	10.93	9.32
EF	0.59	0.59	0.81	0.64	0.65	1.26	1.42	1.21
Co (ppm)	19	59.08	30.04	29.01	30.34	47.51	31.11	29.66
(Co/Al)*104	2.1	7.30	3.54	3.44	3.66	11.57	5.95	5.07
EF		3.48	1.69	1.64	1.74	5.51	2.83	2.42
Cu (ppm)	45	39.01	72.07	32.86	38.02	34.75	75.20	54.90
(Cu/Al)*104	5.1	4.82	8.49	3.90	4.58	8.46	14.39	9.39
EF		0.95	1.67	0.76	0.90	1.66	2.82	1.84
Zn (ppm)	95	184.82	336.85	354.01	218.42	263.23	374.79	222.20
(Zn/Al)*104	11	22.85	39.69	42.01	26.32	64.09	71.71	38.02
EF		2.08	3.61	3.82	2.39	5.83	6.52	3.46
V (ppm)	130	55.22	107.15	98.92	95.68	93.75	105.60	103.66
(V/Al)*104	15	0.68	1.26	1.17	1.15	2.28	2.02	1.77
EF		0.05	0.08	0.08	0.08	0.15	0.13	0.12
Cr (ppm)	90	168.83	282.78	456.95	316.78	278.54	413.02	193.70
(Cr/Al)*104	10.2	20.87	33.32	54.23	38.18	67.81	79.02	33.14
EF		2.05	3.27	5.32	3.74	6.65	7.75	3.25
Ba (ppm)	580	1248.17	1150.91	4258.03	4015.67	3826.19	18,872.96	5193.40
(Ba/Al)*104	66	154.31	135.61	505.35	483.96	931.54	3610.98	888.61
EF		2.34	2.05	7.66	7.33	14.11	54.71	13.46

Table 1. (Continued).

Element	WSA	10,290–10,380 ft	10,380–10,470 ft	10,470–10,560 ft	10,560–10,650 ft	10,650–10,740 ft	10,740–10,830 ft	10,830–10,920 ft
Rb (ppm)	140	35.49	63.37	64.55	64.09	60.71	61.74	59.05
(Rb/Al)*104	16	4.39	7.47	7.66	7.72	14.78	11.81	10.10
EF		0.27	0.47	0.48	0.48	0.92	0.74	0.63
Sr (ppm)	300	124.35	236.67	249.57	217.20	200.15	524.14	260.04
(Sr/Al)*104	34	15.37	27.89	29.62	26.18	48.73	100.28	44.49
EF		0.45	0.82	0.87	0.77	1.43	2.95	1.31
Zr (ppm)	160	168.12	288.00	310.47	264.10	302.52	229.66	278.13
(Zr/Al)*104	18	20.78	33.93	36.85	31.83	73.65	43.94	47.59
EF		1.15	1.89	2.05	1.77	4.09	2.44	2.64
Pb (ppm)	22	23.92	42.81	37.66	46.27	37.02	95.92	43.54
(Pb/Al)*104	2.5	2.96	5.04	4.47	5.58	9.01	18.35	7.45
EF		1.18	2.02	1.79	2.23	3.61	7.34	2.98
U (ppm)	3.7	1.51	2.87	2.90	2.69	2.60	2.52	2.73
(U/Al)*104	0.42	0.19	0.34	0.34	0.32	0.63	0.48	0.47
EF		0.45	0.81	0.82	0.77	1.50	1.15	1.11
Mo (ppm)	1	9.84	12.28	6.18	5.44	4.32	30.54	26.61
(Mo/Al)*104	0.1	1.22	1.45	0.73	0.66	1.05	5.84	4.55
EF		12.16	14.47	7.33	6.56	10.51	58.42	45.52
Y (ppm)	41	12.09	29.33	25.78	25.26	24.02	24.95	26.35
(Y/Al)*104	4.6	1.49	3.46	3.06	3.04	5.85	4.77	4.51
EF		0.32	0.75	0.67	0.66	1.27	1.04	0.98

Table 2. Major element (wt. %) and trace element (mg/kg) abundances of Agbada Formation sediments and world shale average (WSA). *nd*: Not determined.

Element	Al_2O_3	CaO	Cr_2O_3	Fe_2O_3	K_2O	MgO	MnO	Na_2O	P_2O_5	SiO_2	TiO_2	LOI	Total	As	Ni
WSA	16.7	2.20	*nd*	6.90	3.60	2.60	*nd*	1.60	0.16	58.90	0.78	*nd*	93.44	10	68
9660–9750 ft	15.68	1.51	0.02	7.31	1.59	1.16	0.05	0.55	0.22	58.80	0.95	10.93	98.76	*nd*	46.25
9750–9840 ft	7.76	1.12	0.02	4.40	0.91	0.76	0.03	0.30	0.13	76.21	0.50	7.52	99.66	*nd*	32.92
9840–9930 ft	9.87	0.87	0.02	4.40	0.99	0.79	0.03	0.36	0.12	73.20	0.61	8.23	99.50	*nd*	30.60
9930–10,020 ft	11.04	1.22	0.03	5.35	1.16	0.91	0.04	0.46	0.12	68.23	0.69	9.42	98.68	*nd*	36.28
10,020–10,110 ft	2.18	0.42	0.01	1.50	0.47	0.30	0.01	0.11	0.03	92.02	0.19	2.40	99.63	*nd*	18.17
10,110–10,200 ft	6.40	1.35	0.01	3.10	1.00	0.79	0.02	0.29	0.07	78.07	0.47	6.64	98.21	*nd*	23.77
10,200–10,290 ft	5.31	0.82	0.01	2.57	0.80	0.53	0.02	0.23	0.07	82.41	0.35	6.21	99.32	*nd*	19.77
10,290–10,380 ft	6.86	1.45	0.03	4.55	1.05	0.82	0.03	0.31	0.11	74.69	0.43	8.31	98.63	*nd*	36.60
10,380–10,470 ft	15.92	2.51	0.02	8.73	1.61	1.25	0.06	0.60	0.19	48.78	0.89	16.48	97.04	*nd*	52.90
10,470–10,560 ft	16.79	3.03	0.04	8.53	1.66	1.49	0.07	0.66	0.27	48.36	1.00	15.58	97.49	*nd*	41.83
10,560–10,650 ft	15.75	2.37	0.06	6.78	1.72	1.37	0.04	0.67	0.17	50.52	0.94	17.13	97.52	*nd*	41.82
10,650–10,740 ft	15.42	1.37	0.04	6.72	1.69	1.25	0.04	0.56	0.16	57.58	0.86	12.46	98.15	*nd*	39.77
10,740–10,830 ft	15.28	1.18	0.04	5.88	1.65	1.05	0.04	0.56	0.14	60.31	0.90	11.51	98.52	*nd*	57.15
10,830–10,920 ft	16.03	3.06	0.03	8.73	1.72	1.31	0.06	0.55	0.19	47.04	0.87	13.19	92.79	*nd*	54.48
Element	Mn	U	Mo	V	Cr	Co	Ba	Sr	Y	Zr	La	Rb	Cu	Zn	Pb
WSA	850	3.7	1	130	90	19	580	300	41	160	41	140	45	95	22
9660–9750 ft	75.59	2.56	13.30	99.13	142.85	35.22	896.83	180.24	23.22	236.75	51.28	61.60	40.97	163.73	23.48
9750–9840 ft	144.61	1.78	10.68	57.92	150.93	125.82	1063.47	114.33	13.12	185.52	27.96	31.90	32.68	170.23	15.96
9840–9930 ft	145.28	1.96	7.77	66.57	135.35	51.60	515.00	113.34	15.40	195.99	33.75	36.73	23.53	196.74	23.69
9930–10,020 ft	213.04	2.07	12.86	74.24	196.18	53.42	556.06	124.33	17.38	208.18	37.37	41.58	37.58	280.27	35.42
10,020–10,110 ft	523.07	0.76	4.94	25.74	46.71	149.73	766.98	57.11	3.60	147.83	7.41	14.02	17.07	77.06	17.70
10,110–10,200 ft	320.91	1.59	5.69	50.14	100.47	104.40	3455.12	150.23	10.82	250.34	24.10	32.27	29.29	165.94	21.82
10,200–10,290 ft	271.2	1.20	4.70	42.55	98.93	89.31	979.62	87.92	8.67	179.02	17.73	25.40	18.18	106.12	18.74
10,290–10,380 ft	274.14	1.51	9.84	55.22	168.83	59.08	1248.17	124.35	12.09	168.12	24.63	35.49	39.01	184.82	23.92
10,380–10,470 ft	470.64	2.87	12.28	107.15	282.78	30.04	1150.91	236.67	29.33	288.00	58.20	63.37	72.07	336.85	42.81
10,470–10,560 ft	452.8	2.90	6.18	98.92	456.95	29.01	4258.03	249.57	25.78	310.47	53.40	64.55	32.86	354.01	37.66
10,560–10,650 ft	413.91	2.69	5.44	95.68	316.78	30.34	4015.67	217.20	25.26	264.10	51.78	64.09	38.02	218.42	46.27
10,650–10,740 ft	232.35	2.60	4.32	93.75	278.54	47.51	3826.19	200.15	24.02	302.52	50.51	60.71	34.75	263.23	37.02
10,740–10,830 ft	213.23	2.52	30.54	105.60	413.02	31.11	18872.96	524.14	24.95	229.66	50.08	61.74	75.20	374.79	95.92
10,830–10,920 ft	280.62	2.73	26.61	103.66	193.70	29.66	5193.40	260.04	26.35	278.13	50.81	59.05	54.90	222.20	43.54

rocks. Rare earth element mobilization can occur during chemical weathering of bedrock, and source bedrock REE signatures are preserved in the weathering profile because there is no net loss of REE abundance (Condie et al., 1991; Cullers et al., 2000; Kutterolf et al., 2008). Therefore, REE ratios such as La/Yb, Gd/Yb, La/Sm, and Eu/Eu*(where Eu* = europium anomalies) of sediments are considered to be similar to provenance and are usually used to determine bulk source composition (Kutterolf et al., 2008; Dabard and Loi, 2012). REE patterns and Th data of the investigated Agbada Formation sediments indicate the felsic composition of source rocks.

Trace element ratios like Ni/Co, V/Cr, Cu/Zn, and U/Th were used to evaluate paleoredox conditions (Hallberg, 1976; Jones and Manning, 1994). The ratio of uranium to thorium may be used as a redox indicator with the U/Th ratio being higher in organic-rich mudstones (Jones and Manning, 1994). U/Th ratios below 1.25 suggest oxic conditions of deposition, whereas values above 1.25 indicate suboxic and anoxic conditions (Dill et al., 1988;

Table 3. Trace and rare earth element ratios of the studied Agbada Formation sediments.

Sample name	Ni/Co	V/Cr	U/Th	Cr/Ni	V/Sc	La/Sc	La/Yb	Gd/Yb	La/Th	La/Sm	Th/Yb
9660–9750 ft	1.31	0.69	0.19	3.09	5.80	3.00	22.69	3.07	3.84	6.13	5.91
9750–9840 ft	0.26	0.38	0.23	4.58	3.92	1.89	21.13	2.84	3.62	6.23	5.83
9840–9930 ft	0.59	0.49	0.21	4.42	4.27	2.17	21.22	2.82	3.71	6.55	5.72
9930–10,020 ft	0.68	0.38	0.20	5.41	4.74	2.39	21.54	2.82	3.59	6.12	5.99
10,020–10,110 ft	0.12	0.55	0.33	2.57	1.98	0.57	13.81	1.96	3.17	6.31	4.35
10,110–10,200 ft	0.23	0.50	0.23	4.23	3.61	1.73	19.56	2.54	3.49	6.27	5.60
10,200–10,290 ft	0.22	0.43	0.26	5.00	3.18	1.32	20.27	2.74	3.77	6.62	5.37
10,290–10,380 ft	0.62	0.33	0.22	4.61	4.01	1.79	19.23	2.76	3.55	5.68	5.42
10,830–10,920 ft	1.76	0.38	0.19	5.35	6.45	3.51	20.07	2.87	3.84	5.83	5.23
10,380–10,470 ft	1.44	0.22	0.19	10.93	6.30	3.40	20.34	2.78	3.58	6.13	5.68
10,470–10,560 ft	1.38	0.30	0.18	7.57	5.90	3.19	19.46	2.81	3.55	5.80	5.48
10,560–10,650 ft	0.84	0.34	0.18	7.00	5.61	3.02	19.65	2.58	3.53	6.03	5.57
10,650–10,740 ft	1.84	0.26	0.18	7.23	6.72	3.19	21.31	3.07	3.56	5.73	5.99
10,740–10,830 ft	1.84	0.54	0.19	3.56	6.48	3.18	19.58	2.83	3.62	5.68	5.41
Minimum	0.12	0.22	0.18	2.57	1.98	0.57	13.81	1.96	3.17	5.68	4.35
Maximum	1.84	0.69	0.33	10.93	6.72	3.51	22.69	3.07	3.84	6.62	5.99
Average	0.94	0.41	0.21	5.40	4.93	2.45	19.99	2.75	3.60	6.08	5.54
Standart deviation	0.64	0.13	0.04	2.18	1.46	0.90	2.04	0.27	0.17	0.30	0.42

Table 3. (Continued).

Sample name	Th/U	U/Pb	Eu/Eu*	V/Ni	Cr/Th	Th/Co	Th/Cr	Cu/Zn	Th/Sc	V/(Ni+V)
9660–9750 ft	5.23	0.11	0.72	2.14	10.70	0.38	0.09	0.25	0.78	0.68
9750–9840 ft	4.35	0.11	0.67	1.76	19.56	0.06	0.05	0.19	0.52	0.64
9840–9930 ft	4.65	0.08	0.68	2.18	14.87	0.18	0.07	0.12	0.58	0.69
9930–10,020 ft	5.03	0.06	0.71	2.05	18.87	0.19	0.05	0.13	0.66	0.67
10,020–10,110 ft	3.07	0.04	0.78	1.42	20.00	0.02	0.05	0.22	0.18	0.59
10,110–10,200 ft	4.34	0.07	0.78	2.11	14.56	0.07	0.07	0.18	0.50	0.68
10,200–10,290 ft	3.91	0.06	0.72	2.15	21.05	0.05	0.05	0.17	0.35	0.68
10,290–10,380 ft	4.58	0.06	0.73	1.51	24.34	0.12	0.04	0.21	0.50	0.60
10,830–10,920 ft	5.28	0.07	0.68	2.03	18.65	0.50	0.05	0.21	0.91	0.67
10,380–10,470 ft	5.14	0.08	0.70	2.37	30.64	0.51	0.03	0.09	0.95	0.70
10,470–10,560 ft	5.43	0.06	0.71	2.29	21.74	0.48	0.05	0.17	0.90	0.70
10,560–10,650 ft	5.51	0.07	0.73	2.36	19.47	0.30	0.05	0.13	0.86	0.70
10,650–10,740 ft	5.59	0.03	0.87	1.85	29.32	0.45	0.03	0.20	0.90	0.65
10,740–10,830 ft	5.15	0.06	0.71	1.90	13.80	0.47	0.07	0.25	0.88	0.66
Minimum	3.07	0.03	0.67	1.42	10.70	0.02	0.03	0.09	0.18	0.59
Maximum	5.59	0.11	0.87	2.37	30.64	0.51	0.09	0.25	0.95	0.70
Average	4.80	0.07	0.73	2.01	19.83	0.27	0.05	0.18	0.68	0.66
Standart deviation	0.71	0.02	0.05	0.29	5.60	0.19	0.02	0.05	0.24	0.04

Nath et al., 1997; Jones and Manning, 1994). The studied sediments show low U/Th ratios (~0.18–0.33; average = 0.21) (Tables 3 and 4), which imply that the Agbada Formation sediments were deposited in an oxygenated bottom water condition. Th/U ratios in the sediments range between ~5.59 and 3.07 with an average value of ~4.80, which indicates oxidizing conditions. Th/U ratios are high in oxidizing conditions and low in reducing conditions (Kimura and Watanabe, 2001).

A few authors have used the V/Cr ratio as an indicator of bottom water oxygenated condition (Bjorlykke, 1974; Shaw et al., 1990; Nagarajan et al., 2007). Chromium is mainly incorporated in the detrital fraction of sediments and it may substitute for Al in the structure of clays (Bjorlykke, 1974). Vanadium may be bound to organic matter by the amalgamation of V^{4+} into porphyrins, and it is normally found in sediments deposited in reducing environments (Shaw et al., 1990; Kimura and Watanabe, 2001). V/Cr ratios above 2 indicate anoxic conditions, whereas values below 2 imply oxic conditions (Jones and Manning, 1994). The V/Cr ratios in Agbada Formation sediments range from ~0.22 to 0.69, with an average value of ~0.41 (Tables 3 and 4), which indicates that Agbada Formation sediments were deposited in an oxic depositional condition. Numerous authors have used the Ni/Co ratio as a redox indicator (Bjorlykke, 1974; Brumsack, 2006; Nagarajan et al., 2007). Ni/Co ratios below 5 indicate oxic environments, whereas ratios above 5 suggest suboxic and anoxic environments (Jones and Manning, 1994). The Ni/Co ratios vary between ~0.12 and 3.58 with an average value of ~1.11 (Table 2), implying that Agbada Formation sediments were deposited in a well-oxygenated bottom water condition. The Cu/Zn ratio is also used as a redox parameter (Hallberg, 1976). High Cu/Zn ratios indicate reducing depositional conditions, while low Cu/Zn ratios suggest oxidizing conditions (Hallberg, 1976). Consequently, the low Cu/Zn ratios vary between ~0.05 and 0.22 with an average value of ~0.17 in the studied Agbada Formation sediments (Tables 3 and 4), suggesting sediment deposition under oxic conditions. V/(Ni+V) ratios below 0.46 indicate oxic environments, but ratios above 0.54 to 0.82 suggest suboxic and anoxic environments (Hatch and Levanthal, 1992). The V/(Ni + V) ratios in the Agbada Formation sediments encountered at the KR-1 well vary between ~0.59 and 0.70 with an average value of ~0.66, which suggests that there might be rare occurrence of suboxic to anoxic environments of deposition. V/Sc ratios below 9.1 indicate an oxic environment of deposition (Hetzel et al., 2009). The V/Sc ratios in the Agbada Formation sediments vary between ~1.98 and 6.72 with an average value of ~4.93, which indicates an oxic environment of deposition (Tables 3 and 4). Based on REE studies of the early Cretaceous sediments, numerous geoscientists convincingly argued that the REE patterns (including Eu* anomalies), though mostly dependent on their provenance, can also be controlled by fO_2 and sedimentary environment (Ganai and Rashid, 2015). They observed that when fO_2 is low (a reducing environment), the sediments deposited should be characterized by low REE values and a positive europium anomaly (Eu*), whereas sediments deposited in oxidizing conditions (i.e. fO_2 is high) should be characterized by high total REE and Eu depletion (Ganai and Rashid, 2015). As a result, it appears that the Agbada Formation sediments recovered from the KR-1 well, which are characterized by high total REEs and strong negative Eu anomaly, were deposited in an oxidizing environment.

4.6. Rare earth element geochemistry

A comparison of the REE contents in this study and a number of works on the behavior of REEs in secondary environments is shown in Table 5. Standards that are normally used include the world shale average (WSA), as calculated by Piper (1974) from published analyses (Haskin and Haskin, 1964; Wedepohl, 1995); the North American Shale Composite (NASC), analyzed by Gromet et al. (1984); the Upper Continental Crust (UCC), with several slightly different values reported by several authors (e.g., Wedepohl, 1969–1978; McLennan,

Table 4. Some trace element ratios to evaluate paleoredox conditions.

Element ratios	Oxic	Dysoxic	Suboxic to anoxic	Euxinic
Ni/Co[1]	<5	5–7	>7	
V/Cr[1]	<2	2–4.25	>4.25	
U/Th[1]	<0.75	0.75–1.25	>1.25	
V/(Ni + V)[2]	<0.46	0.46–0.60	0.54–0.82	>0.84
V/Sc[3]	<9.1			

[1] Jones and Manning, 1994; [2] Hatch and Levantal, 1992; [3]Akinyemi et al., 2013; Adebayo et al., 2015a.

Table 5. Comparison of normalized rare earth element (REE) contents with literature data.

Element	WSA	UCC	PAAS	NASC	Aver. chondrites	9660–9750 ft	9750–9840 ft	9840–9930 ft	9930–10,020 ft	10,020–10,110 ft	10,110–10,200 ft	10,200–10,290 ft
La	41	30	38.20	31.1	0.32	51.28	27.96	33.75	37.37	7.41	24.10	17.73
Ce	83	64	79.60	66.7	0.90	107.79	58.13	69.52	76.76	17.01	50.37	38.19
Pr	10.1	7.1	8.83	7.7	0.13	11.96	6.44	7.62	8.69	1.81	5.41	4.15
Nd	38	26	33.90	27.4	0.57	45.28	24.23	28.35	32.30	5.98	20.60	15.02
Sm	75	4.5	5.55	5.59	0.21	8.37	4.49	5.16	6.11	1.18	3.84	2.68
Eu	1.61	0.88	1.08	1.18	0.07	1.81	0.90	1.07	1.27	0.28	0.88	0.60
Gd	6.35	3.8	4.66	4.9	0.31	6.93	3.76	4.49	4.89	1.05	3.13	2.40
Tb	1.23	0.64	0.77	0.85	0.05	0.90	0.52	0.55	0.64	0.16	0.42	0.28
Dy	5.5	3.5	4.68	4.17	0.30	4.99	2.85	3.35	3.81	0.73	2.30	1.68
Ho	1.34	0.8	0.99	1.02	0.07	0.90	0.53	0.63	0.71	0.15	0.49	0.33
Er	3.75	2.3	2.85	2.84	0.21	2.40	1.48	1.64	1.94	0.42	1.10	0.88
Tm	0.63	0.33	0.41	0.84	0.03	0.35	0.18	0.24	0.26	0.10	0.18	0.14
Yb	3.53	2.2	2.82	3.06	0.18	0.90	0.52	0.55	0.64	0.16	0.42	0.28
Lu	0.61	0.32	0.43	0.46	0.03	0.33	0.19	0.21	0.25	0.08	0.18	0.14
∑REE	271.65	146.37	184.773	157.81	3.393	244.1635	132.155	157.094	175.6255	36.525	113.41	84.49
Element	WSA	UCC	PAAS	NASC	Aver. chondrites	10,290–10,380 ft	10,380–10,470 ft	10,470–10,560 ft	10,560–10,650 ft	10,650–10,740 ft	10,740–10,830 ft	10,830–10,920 ft
La	41	30	38.20	31.1	0.32	24.63	58.20	53.40	51.78	50.51	50.08	50.81
Ce	83	64	79.60	66.7	0.90	52.94	124.13	111.31	109.18	103.82	105.18	107.23
Pr	10.1	7.1	8.83	7.7	0.13	5.79	13.69	12.48	12.35	11.61	11.90	12.12
Nd	38	26	33.90	27.4	0.57	22.76	51.97	47.27	47.16	43.64	45.20	46.62
Sm	75	4.5	5.55	5.59	0.21	4.34	9.98	8.72	8.92	8.38	8.74	8.95
Eu	1.61	0.88	1.08	1.18	0.07	0.94	2.04	1.83	1.90	1.77	2.28	1.88
Gd	6.35	3.8	4.66	4.9	0.31	3.54	8.33	7.31	7.47	6.62	7.22	7.34
Tb	1.23	0.64	0.77	0.85	0.05	0.48	1.12	1.02	1.00	0.94	1.00	0.98
Dy	5.5	3.5	4.68	4.17	0.30	2.49	6.39	5.76	5.46	5.00	5.40	5.70
Ho	1.34	0.8	0.99	1.02	0.07	0.49	1.16	1.01	1.03	0.96	0.99	1.00
Er	3.75	2.3	2.85	2.84	0.21	1.33	3.19	2.78	2.77	2.57	2.47	2.75
Tm	0.63	0.33	0.41	0.84	0.03	0.18	0.43	0.39	0.37	0.36	0.35	0.36
Yb	3.53	2.2	2.82	3.06	0.18	0.48	1.12	1.02	1.00	0.94	1.00	0.98
Lu	0.61	0.32	0.43	0.46	0.03	0.17	0.42	0.36	0.34	0.34	0.34	0.37
∑REE	271.65	146.37	184.77	157.81	3.39	120.52	282.15	254.63	250.72	237.44	242.13	247.07

WSA (Piper, 1974); UCC (Wedepohl, 1969–1978; McLennan, 1989; Rudnick and Gao, 2003); PAAS (McLennan, 2001); NASC (Gromet et al., 1984); average chondrites (Schmidt et al., 1963).

1989; Rudnick and Gao, 2003), but with rather similar interelement concentrations; the Post-Archean Australian Shale (PAAS), proposed by McLennan (2001); and finally an average of chondrites (Schmidt et al., 1963). The concentrations of the REEs in these standards represent two compositional extremes of siliciclastic source-rocks, one felsic (WSA, UCC, PAAS, and NASC) and the second ultramafic (chondrites) (Piper and Bau, 2013).

Table 5 shows that the concentration range of La in Agbada Formation sediments is from ~58.20 to 7.41 ppm with an average value of ~38.50 ppm and standard deviation of ~15.96. The average value of La in Agbada Formation samples is lower than in WSA (Table 5) but higher than those of other standards such UCC, PAAS, NASC, and average chondrites.

Cerium contents in studied samples range between ~124.13 and 17.01 ppm with an average value of ~ 80.82 ppm and standard deviation of ~33.27. The average value of Ce in the studied samples is relatively lower than in WSA and less than that of UCC, PAAS, NASC, and average chondrites. The concentration range of Pr in the studied sediments is between ~13.69 and 1.81 ppm with an average value of ~ 9.00 ppm and standard deviation of ~3.78. The average concentration value of Pr in Agbada Formation samples is less than in WSA but higher than those of other standards. Concentration levels of Nd range from ~51.97 to 5.98 ppm with an average value of ~34.02 ppm and standard deviation of ~14.57. The average concentration level of Nd is less than in WSA but higher than those of other standards.

Concentration levels of Sm in Agbada Formation sediments range from ~9.98 to 1.18 ppm with an average value of ~6.42 and standard deviation of ~2.79. Concentration levels of Eu in the studied samples range between ~2.28 and 0.28 ppm with an average value of ~1.39 ppm and standard deviation of ~0.61. The average concentration of Sm is less than in WSA but higher than those of the other commonly used standards (Table 5).

The concentration levels of Gd range from ~8.33 to 1.05 ppm with an average value of ~5.32 ppm and standard deviation of ~2.28. The average value of Gd in the studied samples is less than in WSA but less high than those of the other commonly used standards. The levels of Tb in Agbada Formation sediments range between ~8.33 and 1.05 ppm with an average value of ~0.72 ppm and standard deviation of ~0.31. The average concentration level of Tb in studied samples is less than in WSA, PAAS, and NASC but higher than in UCC and average chondrites. Concentration levels of Dy in studied samples range between ~6.39 and 0.73 ppm with an average value of ~3.99 ppm and standard deviation of ~1.77. The average value of Dy in Agbada Formation sediments is higher than in UCC and average chondrites but lower than in the other considered standards. The content levels of Ho in studied samples range from ~1.16 to 0.15 ppm with an average value of ~ 0.74 ppm and standard deviation of ~0.31. The average concentration value of Ho in studied samples is less than those of all considered commonly used standards. Concentration levels of Er range from ~3.19 to 0.42 ppm with an average value of ~1.98 ppm and standard deviation of 0.31. The average concentration of Er in studied samples is higher than in average chondrites but lower than in the other standards. Concentration levels of Tm in studied samples range between ~0.43 and 0.10 ppm with an average value of ~0.28 ppm and standard deviation of ~0.11. The average concentration of Tm in studied samples is higher than in average chondrites but lower than in other considered standards. The contents of Yb in Agbada Formation sediments range from ~1.12 to 0.16 ppm with an average value of ~0.72 ppm and standard deviation of ~0.31. The average concentration of Yb in studied samples is higher than in average chondrites but lower than in other considered standards. Contents of Lu in Agbada Formation sediments range from ~0.42 to 0.08 ppm with an average value of ~0.27 ppm and standard deviation of ~0.10. The average concentration level of Lu is higher than in average chondrites but lower than its concentration in other considered standards.

Cerium anomaly may perhaps be quantified by comparing the measured concentration (Ce) with an expected concentration (Ce*) obtained by interpolating between the values of the neighboring elements. Ce anomalies in shales of the anoxic facies are attributed to eustatic sea level changes (Wilde et al., 1996). Similar to Mn, Ce^{4+} is less soluble under oxic conditions, whereas under anoxic conditions it will be mobilized, leading to the depletion in Ce in anoxic sediments relative to those deposited under oxic conditions. A negative Ce anomaly would be indicative of postdepositional remobilization of Ce in the water column.

Table 6 shows two different values given for the Ce anomaly, which are based on different calculations. Taylor and McLennan (1985) suggested the use of the geometric mean $Ce^* = \sqrt{(La^*Pr)}$. The ratio Ce/Ce* is then a measure of the anomaly, with values greater than unity being termed positive. Wilde et al. (1996) promoted the use of the arithmetic mean Ce* = (La+Pr)/2 and calculated the logarithm of the ratio Ce/Ce*. Both calculations lead to the same values as Ce* by KR-1 well samples mostly showing positive anomaly values. Therefore, the Agbada Formation sediments were deposited under oxic conditions, which indicates the incorporation of this cerium from the water column.

5. Conclusions

Lithologically, glauconite and rare pyrite are the most important accessory minerals in the studied well, indicating a slightly anoxic marginal marine environment of deposition while the palynomorph percentage distribution shows that there are more terrestrially derived miospores (dominated by *Zonocostites ramonae*, *Psilatricolporites crassus*, *Arostichum aurium*, and *Laevigatosporites* sp.) than marine phytoplanktons. These indicate that the main

Table 6. Ce anomaly for Agbada Formation sediments (two quantification approaches are given).

Authors	Equations	9660–9750 ft	9750–9840 ft	9840–9930 ft	9930–10,020 ft	10,020–10,110 ft	10,110–10,200 ft	10,200–10,290 ft
Taylor and McLennan (1985)	Ce* = √(La*Pr)	24.76	13.42	16.04	18.02	3.66	11.42	8.57
	Ce/Ce*	4.35	4.33	4.34	4.26	4.64	4.41	4.45
Wilde et al. (1996)	Ce* = (La + Pr)/2	57.26	31.18	37.56	41.71	8.32	26.80	19.80
	Log (Ce/Ce*)	0.64	0.64	0.64	0.63	0.67	0.64	0.65
Authors	Equations	10,290–10,380 ft	10,380–10,470 ft	10,470–10,560 ft	10,560–10,650 ft	10,650–10,740 ft	10,740–10,830 ft	10,830–10,920 ft
Taylor and McLennan (1985)	Ce* = √(La*Pr)	24.63	58.20	53.40	51.78	50.51	50.08	50.81
	Ce/Ce*	2.15	2.13	2.08	2.11	2.06	2.10	2.11
Wilde et al. (1996)	Ce* = (La + Pr)/2	36.95	87.30	80.09	77.66	75.77	75.11	76.22
	Log (Ce/Ce*)	0.33	0.33	0.32	0.32	0.31	0.32	0.32

Ce* = Cerium anomaly.

environment of deposition in the KR-1 well is coastal to marginal marine consisting of coastal deltaic-inner neritic, made up of tidal channel and shoreface deposits (Adeigbe et al., 2013). Geochemical results show that the average concentrations of considered REEs are less than their concentrations in WSA. Trace metal ratios such as Th/Cr, Cr/Th, Th/Co, and Cr/Ni suggest that the sediments were derived from felsic source rocks. REE patterns such as La/Yb, Gd/Yb, La/Sm, and Eu/Eu* and Th data confirmed the felsic composition of the sediments. Ratios of U/Th, Ni/Co, Cu/Zn, and V/Sc indicate well-oxygenated bottom water conditions. Estimated Eu* and Ce* anomalies obtained from the studied samples suggest an oxidizing environment of deposition. Nonetheless, the ratios of V/Cr suggest a range of environmental conditions. Moreover, ratios of V/(Ni+V) suggest rare suboxic to anoxic environments of deposition.

Acknowledgments

The authors sincerely acknowledge the technical assistance of the final-year students who participated in the fieldwork (Sedimentary/Petroleum Geology Option 2012/2013 and 2014/2015 academic sessions). The authors would also like to acknowledge Ms Riana Rossouw, LA-ICP-MS laboratory of the University of Stellenbosch, for multielement analysis.

References

Adebayo OF (2011). Biostratigraphy, Sequence Stratigraphic Analysis of Three Offshore Wells from the Niger Delta, Nigeria. PhD, University of Ado Ekiti, Ado Ekiti, Nigeria.

Adebayo OF, Akinyemi SA, Madukwe HY, Aturamu AO, Ojo AO (2015a). Paleoenvironmental studies of Ahoko Shale, south eastern Bida basin, Nigeria: insight from palynomorph assemblage and trace metal proxies. International Journal of Scientific and Research Publications 5: 1-16.

Adebayo OF, Ojo AO, Aturamu AO (2015b). Foraminiferal and calcareous nannofossil studies of KR-1 well, offshore, Southwest Niger Delta Basin, Nigeria. Elixir Earth Science 79: 30323-30328.

Adeigbe OC, Ola-Buraimo AO, Moronhunkola AO (2013). Palynological characterization of the Tertiary offshore Emi-1 well, Dahomey Basin, Southwestern Nigeria. International Journal of Scientific and Technological Research 2: 58-70.

Adenugba AA, Dipo SO (2013). Non-oil exports in the economic growth of Nigeria: a study of agricultural and mineral resources. J Educ Soc Res 3: 403-418.

Akinyemi SA, Adebayo OF, Ojo OA, Fadipe OA, Gitari, WM (2013). Mineralogy and geochemical appraisal of paleo-redox indicators in Maastrichtian outcrop shales of Mamu Formation, Anambra Basin, Nigeria. J Nat Sci Res 10: 48-64.

Ako BD, Ojo SB, Okereke CS, Fieberg FC, Ajayi TR, Adepelumi AA, Afolayan JFO, Afolabi O, Ogunnusi HO (2004). Some observation from gravity/magnetic data interpretation of the Niger Delta. NAPE Bulletin 17: 4-8.

Algeo TJ, Maynard JB (2004). Trace-element behavior and redox facies in core shales of Upper Pennsylvanian Kansas-type cyclothems. Chem Geol 206: 289-318.

Arnaboldi M, Meyers PA (2003). Geochemical evidence for paleoclimatic variations during deposition of two Late Pliocene sapropels from the Vrica section, Calabria. Palaeo Palaeo Palaeo 190: 257-271.

Barreda VD, Palamarczuk S (2000). Palinomorfos continentales y marinos de la Formación Monte León en su área tipo, provincia de Santa Cruz, Argentina. Ameghiniana 37: 3-12 (in Spanish).

Bjorlykke K (1974). Geochemical and mineralogical influence of Ordovician island arcs on epicontinental clastic sedimentation: a study of Lower Palaeozoic sedimentation in the Oslo region, Norway. Sedimentology 21: 251-272.

Brumsack HJ (1980). Geochemistry of Cretaceous black shales from the Atlantic Ocean (DSDP Legs 11, 14, 36, and 41). Chem Geol 31: 1-25.

Brumsack HJ (1986). The inorganic geochemistry of Cretaceous black shales (DSDP Leg 41) in comparison to modern upwelling sediments from the Gulf of California. In: Summerhayes CP, Shackleton NJ, editors. North Atlantic Palaeoceanography. London, UK: Geological Society of London Special Publications, pp. 447-462.

Brumsack HJ (1989). Geochemistry of recent TOC-rich sediments from the Gulf of California and the Black Sea. Geol Rundsch 78: 851-882.

Brumsack HJ (2006). The trace metal content of recent organic carbon-rich sediments: implications for Cretaceous black shale formation. Palaeo Palaeo Palaeo 232: 344-361.

Calvert SE, Pedersen TF (1993). Geochemistry of recent oxic and anoxic marine sediments: implications for the geological record. Mar Geol 113: 67-88.

Condie KC, Marais DJD, Abbott D (2001). Precambrian superplumes and supercontinents: a record in black shales, carbon isotopes, and paleoclimates. Precambrian Res 106: 239-260.

Condie KC, Wilks M, Rosen DM, Zlobin VL (1991). Geochemistry of metasediments from the Precambrian Hapschan Series, eastern Anabar Shield, Siberia. Precambrian Res 50: 37-47.

Cox R, Lowe DR, Cullers RL (1995). The influence of sediment recycling and basement composition on evolution of mudrock chemistry in the southwestern United States. Geochim Cosmochim Ac 59: 2919-2940.

Crusius J, Calvert S, Pedersen T, Sage D (1996). Rhenium and molybdenum enrichments in sediments as indicators of oxic, suboxic and sulfidic conditions of deposition. Earth Planet Sc Lett 145: 65-78.

Cullers RL (1994). The controls on the major and trace element variation of shales, siltstones and sandstones of Pennsylvanian-Permian age from uplifted continental blocks in Colorado to platform sediment in Kansas, USA. Geochim Cosmochim Ac 58: 4955-4972.

Cullers RL (1995). The controls on the major and trace element evolution of shales, siltstones and sandstones of Ordovician to Tertiary age in the Wet Mountains region, Colorado, U.S.A. Chem Geol 123: 107-131.

Cullers RL (2000). The geochemistry of shales, siltstones and sandstones of Pennsylvanian-Permian age, Colorado, USA: implications for provenance and metamorphic studies. Lithos 51: 305-327.

Cullers RL, Podkovyrov VN (2000). Geochemistry of the Mesoproterozoic Lakhanda shales in southeastern Yakutia, Russia: implications for mineralogical and provenance control, and recycling. Precambrian Res 104: 77-93.

Dabard MP, Loi A (2012). Environmental control on concretion-forming processes: examples from Paleozoic terrigenous sediments of the North Gondwana margin, Amorican Massif (Middle Ordovician and Middle Devonian) and SW Sandinia (Late Ordovician). Sediment Geol 267: 93-103.

Dean WE, Gardner JV, Piper DZ (1997). Inorganic geochemical indicators of glacial-interglacial changes in productivity and anoxia of the California continental margin. Geochim Cosmochim Ac 61: 4507-4518.

Dean WE, Piper DZ, Peterson LC (1999). Molybdenum accumulation in Cariaco basin sediment over the past 24 k.y.: a record of water-column anoxia and climate. Geology 27: 507-510.

Demchuk TD, Moore TA (1993). Palynofloral and organic characteristics of a Miocene bog-forest, Kalimantan, Indonesia. Org Geochem 20: 119-134.

Dill HG, Teshner M, Wehner H (1988). Petrography, inorganic and organic geochemistry of Lower Permian Carboniferous fan sequences (Brandschiefer Series) FRG: constraints to their palaeogeography and assessment of their source rock potential. Chem Geol 67: 307-325.

Durugbo EU (2013). Palynostratigraphy, age determination and depositional environments of Imo Shale Exposures at the Okigwe/Port Harcourt Express Road Junction Okigwe, South-eastern Nigeria. Greener Journal of Physical Science 3: 255-272.

Ejedawe JE (1981). Patterns of incidence of oil reserves in Niger Delta Basin. AAPG Bull 65: 1574-1585.

El-Beialy SY, Mahmoud MS, Ali SA (2005). Insights on the age, climate and environment of the Miocene Rudeis and Kareem formations, GS-78-1 well, Gulf of Suez, Egypt: a palynological approach. Rev Espanola Micropaleont 37: 273-289.

Evamy DD, Haremboure J, Kamerling P, Knaap WA, Mollot FA, Rowlands PH (1978). Hydrocarbon habitat of Tertiary Niger Delta. AAPG Bull 62: 1-39.

Faegri K, Iversen J (1989).Textbook of Pollen Analysis. New York, NY, USA: John Wiley & Sons.

Fayose EA (1970). Stratigraphical paleontology of Afowo-1 well, southern Nigeria. J Min Geol 5: 1-97.

Ganai JA, Rashid SA (2015). Rare earth element geochemistry of the Permo-Carboniferous clastic sedimentary rocks from the Spiti Region, Tethys Himalaya: significance of Eu and Ce anomalies. Chin J Geoch 34: 252-264.

Germeraad JJ, Hopping GA, Muller J (1968). Palynology of Tertiary sediments from tropical areas. Rev Palaeobot Palyno 6: 189-348.

Graham A (1987). Miocene communities and paleoenvironments of southern Costa Rica. Am J Bot 74: 1501-1518.

Gromet PL, Dymektev FP, Haskin LA, Korotev RO (1984). The North American shale composite: its composition, major and minor element characteristics. Geochim Cosmochim Ac 48: 2469-2482.

Hallberg RO (1976). A geochemical method for investigation of palaeoredox conditions in sediments. Ambio Spec Rep 4: 139-147.

Haskin MA, Haskin L (1964). Rare earth elements in European shales: a redetermination. Science 748: 507-509.

Hatch JR, Leventhal JS (1992). Relationship between inferred redox potential of the depositional environment and geochemistry of the Upper Pennsylvanian (Missourian) Stark Shale Member of the Dennis Limestone, Wabaunsee County, Kansas, U.S.A. Chem Geol 99: 65-82.

Hetzel A, Böttcher ME, Wortmann UG, Brumsack H (2009). Paleo-redox conditions during OAE 2 reflected in Demerara Rise sediment geochemistry (ODP Leg 207). Palaeo Palaeo Palaeo 273: 302-328.

Hopping CA (1967). Palynology and the oil industry. Rev Palaeobot Palyno 2: 23-48.

Hospers J (1965). Gravity field and structure of the Niger Delta, Nigeria, West Africa. Geol Soc Am Bull 76: 407-422.

Jones B, Manning DAC (1994). Comparison of geological indices used for the interpretation of palaeoredox conditions in ancient mudstones. Chem Geol 111: 111-129.

Kaplan A, Lusser CU, Norton IO (1994). Tectonic Map of the World, Panel 10. Scale 1:10,000,000. Tulsa, OK, USA: American Association of Petroleum Geologists.

Kimura H, Watanabe Y (2001). Oceanic anoxia at the Precambrian-Cambrian boundary. Geology 21: 995-998.

Knox GJ, Omatsola EM (1987). Development of the Cenozoic Niger Delta in terms of the "Escalator Regression" model and impact on hydrocarbon distribution. In: Proceedings of the KNGMG Symposium: Coastal Lowlands, Geology and Geotechnology. Dordrecht, the Netherlands: Kluwer, pp. 181-202.

Kogbe CA, Sowunmi MA (1980). The age of the Gwandu Formation (Continental Terminal) in North-Western Nigeria. Ann Min Geol 28: 43-53.

Kulke H (1995). Nigeria. In: Kulke H, editor. Regional Petroleum Geology of the World. Part II: Africa, America, Australia and Antarctica. Berlin, Germany: Gebruder Borntraeger, pp. 143-172.

Kutterolf S, Diever R, Schacht U, Krawinkel H (2008). Provenance of the Carboniferous Hodiwipfel Formation (Karawanken Mountains, Austri/Slovenia) geochemistry versus petrography. Sediment Geol 203: 246-266.

Loeblich AR Jr, Tappan H (1964). Treatise on Invertebrate Paleontology, Part C, Protista, Vols. 1 and 2, Sarcodina Chiefly "Thecamoebians" and Foraminiferida. Lawrence, KS, USA: University of Kansas Press.

McLennan SM (1989). Rare earth elements in sedimentary rocks: influence of provenance and sedimentary processes. Rev Miner Geochem 21: 169-200.

McLennan SM (2001). Relationships between the trace element composition of sedimentary rocks and upper continental crust. Geochem Geophy Geosys 2: 1-24.

Morford JL, Russell AD, Emerson S (2001). Trace metal evidence for changes in the redox environment associated with the transition from terrigenous clay to diatomaceous sediment, Saanlich Inlet, BC. Mar Geol 174: 355-369.

Murat RC (1972). Stratigraphy and paleogeography of the Cretaceous and Lower Tertiary in Southern Nigeria, In: Dessauvagie TFJ, Whiteman AJ, editors. African Geology. Ibadan, Nigeria: University of Ibadan, pp. 261-269.

Murray JW (1991). Ecology and Paleontology of Benthic Foraminifera. London, UK: Longman.

Nagarajan R, Madhavaraju J, Nagendral R, Armstrong-Altrin JS, Moutte J (2007). Geochemistry of Neoproterozoic shales of the Rabanpalli Formation, Bhima Basin, Northern Karnataka, southern India: implications for provenance and paleoredox conditions. Rev Mex Cienc Geol 24: 150-160.

Nath BN, Bau M, Rao BR, Rao ChM (1997). Trace and rare earth elemental variation in Arabian Sea sediments through a transect across the oxygen minimum zone. Geochim Cosmochim Ac 61: 2375-2388.

Nwajide CS, Reijers TJA (1996). Sequence architecture in outcrop: examples from the Anambra Basin, Nigeria. NAPE Bulletin 11: 23-32.

Okosun EA, Liebau A (1999). Foraminiferal biostratigraphy of Eastern Niger Delta, Nigeria. NAPE Bulletin 14: 136-156.

Olayiwola PO (1987). Petroleum and Structural Change in a Developing Country: The Case of Nigeria. New York, NY, USA: Praeger.

Pailler D, Bard E, Rostek F, Zheng Y, Mortlock R, van Geen A (2002). Burial of redox-sensitive metals and organic matter in the equatorial Indian Ocean linked to precession. Geochim Cosmochim Ac 66: 849-865.

Palamarczuk S, Barreda VD (1998). Bioestratigrafia de dinoflagelados de la Formacion Chenque (Mioceno), provincia del Chubut. Ameghiniana 35: 415-426 (in Spanish).

Petters SW (1979a). Nigerian Paleocene benthonic foraminiferal biostratigraphy, paleoecology and paleobiologeography. Mar Micropaleontol 4: 85-99.

Petters SW (1979b). Some Late Tertiary foraminifera from parabe-1 well, Eastern Niger Delta. Rev Esp Micropaleontol 11: 1190-133.

Petters SW (1982). Central West African Cretaceous-Tertiary benthic foraminifera and stratigraphy. Palaeontographica Abt A 179: 1-104.

Piper DZ (1974). Rare-earth elements in the sedimentary cycle: a summary. Chem Geol 14: 285-304.

Piper DZ (1994). Seawater as the source of minor elements in black shales, phosphorites and other sedimentary rocks. Chem Geol 114: 95-114.

Piper DZ, Bau M (2013). Normalized rare earth elements in water, sediments, and wine: identifying sources and environmental redox conditions. American Journal of Analytical Chemistry 4: 69-83.

Postuma JA (1971). Manual of Planktonic Foraminifera. New York, NY, USA: Elsevier Publishing.

Reijers TJA, Petters SW, Nwajide CS (1997). The Niger Delta Basin. In: Selley RC, editor. African Basins-Sedimentary Basin of the World 3. Amsterdam, the Netherlands: Elsevier Science, pp. 151-172.

Rimmer SM (2004). Geochemical paleoredox indicators in Devonian–Mississippian black shales, Central Appalachian Basin (USA). Chem Geol 206: 373-391.

Rudnick RL, Gao S (2003). Composition of the continental crust. In: Holland HD, Turekian KK, editors. Treatise on Geochemistry. New York, NY, USA: Elsevier, pp. 1-64.

Sarjeant WAS (1974). English Jurassic dinoflagellate cysts and acritarch: a re-examination of some type and figure specimen. Geosci Man 1: 1-25.

Schmidt RA, Smith RH, Lasch JE, Mosen AW, Olehy DA, Vasilevshis J (1963). Abundances of fourteen rare-earth elements, scandium, and yttrium in meteoritic and terrigenous matter. Geochim Cosmochim Ac 27: 577-622.

Selley RC (1976). An Introduction to Sedimentology. London, UK: Academic Press.

Shaw TJ, Geiskes JM, Jahnke RA (1990). Early diagenesis in differing depositional environments: the response of transition metals in pore water. Geochim Cosmochim Ac 54: 1233-1246.

Short KC, Stauble AJ (1967). Outline of geology of Niger Delta. AAPG Bull 51: 761-779.

Simmons MD, Bidgood MD, Brenac P, Crevello PD, Lambiase JJ, Morley CK (1999). Microfossil assemblages as proxies for precise palaeoenvironmental determination – an example from Miocene sediments of northwest Borneo. In: Jones RW, Simmons MD, editors. Biostratigraphy in Production and Development Geology. London, UK: Geological Society of London Special Publications, pp. 219-241.

Stacher P (1995) Present understanding of the Niger Delta hydrocarbon habitat. In: Oti MN, Postma G, editors. Geology of Deltas. Rotterdam, the Netherlands: AA Balkema, pp. 257-267.

Thanikaimoni G (1987). Mangrove Palynology. Pondicherry, India: Institut francais de Pondichery, Travaux de la Section Scientifique et Technique.

Tomlinson PB (1986). The Botany of Mangroves. Cambridge, UK: Cambridge University Press.

Turekian KK, Wedepohl KH (1961). Distribution of the elements in some major units of the Earth's crust. Geol Soc Am Bull 72: 175-192.

Warning B, Brumsack HJ (2000). Trace metal signatures of eastern Mediterranean sapropels. Palaeo Palaeo Palaeo 158: 293-309.

Weber KJ, Daukoru EM (1975). Petroleum geological aspects of the Niger Delta. J Min Geol 12: 9-32.

Wedepohl KH (1969–1978). Handbook of Geochemistry, I–IV. Berlin, Germany: Springer-Verlag.

Wedepohl KH (1971). Environmental influences on the chemical composition of shales and clays. In: Ahrens LH, Press F, Runcorn SK, Urey HC, editors. Physics and Chemistry of the Earth. Oxford, UK: Pergamon, pp. 305-333.

Wedepohl KH (1991). The composition of the upper earth's crust and the natural cycles of selected metals. Metals in natural raw materials. In: Merian E, editor. Metals and Their Compounds in the Environment. Weinheim, Germany: VCH, pp. 3-17.

Wedepohl WE (1995). The composition of the continental crust. Geochim Cosmochim Ac 59: 1217-1232.

Wilde P, Quinby-Hunt MS, Erdtmann BD (1996). The whole-rock cerium anomaly: a potential indicator of eustatic sea-level changes in shales of the anoxic facies. Sediment Geol 101: 43-53.

Wood GD, Gabriel AM, Lawson JC (1996). Palynological techniques - processing and microscopy. In: Jansonius J, McGregor V, editors. Palynology: Principles and Applications. Dallas, TX, USA: American Association of Stratigraphic Palynologists, pp. 29-50.

Wronkiewicz DJ, Condie KC (1990). Geochemistry and mineralogy of sediments from the Ventersdorp and Transvaal Supergroups, South Africa: Cratonic evolution during the early Proterozoic. Geochim Cosmochim Ac 54: 343-354.

Yarincik KM, Murray RW, Lyons TW, Peterson LC, Haug GH (2000). Oxygenation history of bottom waters in the Cariaco Basin, Venezuela, over the past 578,000 years: results from redox-sensitive metals (Mo, V, Mn, and Fe). Paleoceanography 15: 593-604.